International Journal of Solids and Structures 50 (2013) 578–587

Contents lists available at SciVerse ScienceDirect

International Journal of Solids and Structures

journal homepage: www.elsevier.com/locate/ijsolstr

Swell-induced surface instability of hydrogel layers with material properties varying in thickness direction

Zhigen Wu [a], Nikolaos Bouklas [b], Rui Huang [b,*]

[a] School of Civil Engineering, Hefei University of Technology, Hefei, Anhui 230009, China
[b] Department of Aerospace Engineering and Engineering Mechanics, University of Texas, Austin, TX 78712, USA

ARTICLE INFO

Article history:
Received 27 July 2012
Received in revised form 2 October 2012
Available online 9 November 2012

Keywords:
Hydrogel
Surface instability
Creasing
Wrinkling

ABSTRACT

Upon swelling in a solvent, a thin hydrogel layer on a rigid substrate may become unstable, developing various surface patterns. Recent experimental studies have explored the possibilities to generate controllable surface patterns by chemically modifying the molecular structures of the hydrogel near the surface. In this paper, we present a theoretical stability analysis for swelling of hydrogel layers with material properties varying in the thickness direction. As a specialization of the general procedure, hydrogel bilayers with different combinations of the material properties are examined in details. For a soft-on-hard bilayer, the onset of surface instability is determined by the short-wave limit, similar to a homogeneous layer. In contrast, for a hard-on-soft bilayer, a long-wave mode with a finite wavelength emerges as the critical mode at the onset of surface instability, similar to wrinkling of an elastic thin film on a compliant substrate, and the critical swelling ratio is much lower than that for a homogeneous hydrogel layer. A smooth transition of the critical mode is predicted as the volume fraction of the top layer changes, linking surface instability of a homogeneous layer to thin film wrinkling as two limiting cases. The results from the present study suggest that both the critical condition and the instability mode depend sensitively on the variation of the material properties in the thickness direction of the hydrogel layer.

1. Introduction

A hydrogel swells significantly when imbibing a large amount of solvent (e.g., water). Swell-induced surface instability of hydrogels has been observed by many (e.g., Southern and Thomas, 1965; Tanaka et al., 1987, 1992; Sultan and Boudaoud, 2008; Trujillo et al., 2008; Guvendiren et al., 2009; Dervaux et al., 2011; Velankar et al., 2012). A number of theoretical and numerical studies have also been reported (Onuki, 1989; Hong et al., 2009b; Kang and Huang, 2010a,b,c; Wong et al., 2010; Dervaux and Ben Amar, 2011; Cao et al., 2012). Most of the theoretical studies to date have assumed the hydrogel to be homogeneous before swelling. Recently, a series of experiments by Guvendiren et al. (2009, 2010a,b) have observed a rich variety of surface patterns (including creases and wrinkles) by using hydrogels with depth-wise crosslink gradients. In their experiments, poly(hydroxyethyl methacrylate) (PHEMA) hydrogel layers were fabricated from a UV-curable precursor solution composed of partially polymerized PHEMA, a photo-initiator, and a crosslinker (ethylene glycol dimethacrylate, EGDMA). The precursor solution was spin-coated onto a rigid substrate (silicon or glass) and exposed to UV light to form a crosslinked layer. In the presence of oxygen, a depth-wise crosslink gradient was generated due to oxygen inhibition of the radical polymerization near the surface. The gradient profile of the crosslink density can be modulated by the initiator and crosslinker concentration, UV exposure intensity and time, and the layer thickness. When exposed to water, the hydrogel layer swelled and distinctive surface patterns formed. It was found that both the critical condition and the characteristic length scale of the surface patterns depended on the crosslink gradient. Motivated by these experiments, we present a theoretical analysis on swell-induced surface instability of hydrogel layers with material properties varying in the thickness direction.

The critical condition for the onset of swell-induced surface instability in hydrogels has been an interesting subject of theoretical studies recently. A closely related problem was considered by Biot (1963), who predicted the critical compressive strain for wrinkle-like surface instability of a hyperelastic half-space, independent of the material property. However, Gent and Cho (1999) found that Biot's prediction considerably overestimated the critical strain in their experiments with rubber blocks compressed by bending, in which they observed surface creases. Unlike wrinkling, creasing is highly localized with large deformation. By an energetic consideration, Hong et al. (2009b) predicted a critical strain for surface creasing of an elastomer, considerably lower than Biot's

* Corresponding author.
E-mail address: ruihuang@mail.utexas.edu (R. Huang).

0020-7683/$ - see front matter © 2012 Elsevier Ltd. All rights reserved.
http://dx.doi.org/10.1016/j.ijsolstr.2012.10.022

prediction. More recently, Cao and Hutchinson (2012a) showed that surface wrinkling in an elastomer is highly unstable and extremely sensitive to imperfections that could significantly reduce the critical strain. Based on a nonlinear post-bifurcation analysis and numerical simulations, they concluded that a tiny initial imperfection can trigger the wrinkling instability to collapse into a localized crease. For a hydrogel layer on a rigid substrate, the critical condition for swell-induced surface instability is similar to the elastomers under compression, but with subtle differences due to the interaction between solvent and the polymer network. Following a procedure similar to Biot's linear perturbation analysis, Kang and Huang (2010b) predicted that the critical swelling ratio for wrinkling instability of a hydrogel layer varies over a wide range, depending on the material parameters (both the polymer network and the solvent). In contrast, the critical compressive strain for an elastomer is independent of the material parameter by Biot's analysis. Again, based on the energetic consideration and numerical calculations, Weiss et al. (Submitted for publication) found that the critical swelling ratio for onset of surface creasing is considerably lower than that for wrinkling. Similar to surface wrinkling of an elastomer, swell induced surface wrinkling in hydrogels is expected to be highly unstable and sensitive to imperfections, although theoretical analysis of this kind has not been reported to the best of our knowledge. On the other hand, a wide range of critical swelling ratios have been reported from various experiments (Southern and Thomas, 1965; Tanaka et al., 1987,1992; Trujillo et al., 2008). Direct comparison between experiments and theoretical predictions has been scarce.

The theoretical studies predict no characteristic length scale for the surface instability (wrinkling and creasing) in homogeneous elastomers and hydrogels. By including the effect of surface tension, Kang and Huang (2010c) predicted a characteristic wrinkle wavelength that scales almost linearly with the thickness of the hydrogel layer. Similar analyses with the surface tension effect were carried out by Ben Amar and coworkers (Ben Amar and Ciarletta, 2010; Dervaux and Ben Amar, 2011) using a volume growth model. Alternatively, a characteristic length scale may be introduced by assuming a thin skin layer at the surface of the hydrogel (Hohlfeld and Mahadevan, 2011) or more generally, by assuming a gradient of the material properties in the thickness direction. In this paper, we present a linear stability analysis for swelling of hydrogel layers with material properties varying in the thickness direction. As a specialization of the general procedure, hydrogel bilayers with different combinations of the material properties are examined in details. The results suggest that both the critical condition and the characteristic length depend sensitively on the depth-wise variation of the material properties in the hydrogel layer.

The remainder of this paper is organized as follows. Section 2 briefly reviews a nonlinear field theory for hydrogels and presents the transversely homogeneous solution for swelling of hydrogel layers. A linear perturbation analysis is performed in Section 3, followed by a bilayer model in Section 4. The theoretical results are discussed in Section 5, in comparison with the previous studies. Two numerical examples are presented to highlight the distinct surface instability behaviors for two types of hydrogel bilayers. We conclude with a short summary in Section 6.

2. Constrained swelling of hydrogel layers

In this section we briefly review the nonlinear theory of polymer gels (Hong et al., 2008, 2009a; Kang and Huang, 2010a) and present a transversely homogeneous solution for swelling of a hydrogel layer with material properties varying in the thickness direction.

2.1. A nonlinear field theory

Consider a hydrogel immersed in a solvent. The free energy density of the hydrogel locally depends on both the elastic deformation of the polymer network and the concentration of solvent molecules, which is taken as

$$U(\mathbf{F}, C) = U_e(\mathbf{F}) + U_m(C), \tag{1}$$

where $\mathbf{F}$ is the deformation gradient tensor of the polymer network, C the nominal concentration of solvent molecules. The two free energy terms, due to elastic deformation and polymer/solvent mixing, respectively, take the form:

$$U_e(\mathbf{F}) = \frac{1}{2}NkT(I - 3 - 2\log J), \tag{2}$$

$$U_m(C) = \frac{kT}{\Omega}\left(\Omega C \log\frac{\Omega C}{1+\Omega C} + \frac{\chi\Omega C}{1+\Omega C}\right), \tag{3}$$

where $I = F_{ij}F_{ij}$ and $J = \det(\mathbf{F})$ are the invariants of the deformation gradient. This free energy function has its root in the statistical mechanics models of rubber elasticity and polymer solution (Flory and Rehner, 1943a,b; Flory, 1942; Huggins, 1941). The polymer network of the hydrogel is characterized by a single parameter, N, as the effective number of polymer chains per unit volume of the dry polymer. The parameter N is determined by the degree of cross-linking; for normal cross-linking (for which four chains meet at each junction) it is simply twice the number of crosslinks per unit volume (Treloar, 1958). The dry polymer network has an initial shear modulus, $G_0 \approx NkT$, where T is the absolute temperature and k the Boltzmann constant. Each of the solvent molecules has the volume Ω. The interaction between the solvent and the polymer is represented by a dimensionless parameter, χ, often referred to as the Flory parameter.

In the equilibrium state, the chemical potential of the solvent is a constant in the hydrogel and equal to that of the external solvent, i.e., $\mu = \hat{\mu}$, while the solvent concentration C as a field quantity may be inhomogeneous. By Legendre transform, the free energy density can be re-written as a function of the deformation gradient and the chemical potential:

$$\hat{U}(\mathbf{F}, \mu) = U(\mathbf{F}, C) - \mu C. \tag{4}$$

Furthermore, assume that both the polymer network and the solvent are incompressible, so that the volume of the hydrogel changes as the solvent concentration changes, namely

$$J = 1 + \Omega C. \tag{5}$$

Combining Eqs. (1)–(5), we obtain

$$\hat{U}(\mathbf{F}, \mu) = \frac{1}{2}NkT(I - 3 - 2\log J) + \frac{kT}{\Omega}\left[(J-1)\log\frac{J-1}{J} + \frac{\chi(J-1)}{J}\right] - \frac{\mu}{\Omega}(J-1). \tag{6}$$

The nominal stress in the hydrogel is then obtained as

$$s_{ij} = \frac{\partial\hat{U}}{\partial F_{ij}} = NkT(F_{ij} + \alpha H_{ij}), \tag{7}$$

where

$$\alpha = -\frac{1}{J} + \frac{1}{N\Omega}\left(\log\frac{J-1}{J} + \frac{1}{J} + \frac{\chi}{J^2} - \frac{\mu}{kT}\right), \tag{8}$$

$$H_{ij} = \frac{1}{2}e_{ijk}e_{JKL}F_{jK}F_{kL}. \tag{9}$$

In the absence of body forces, the mechanical equilibrium requires that

$$\frac{\partial s_{ij}}{\partial X_J} = 0, \tag{10}$$

in the body of the hydrogel, along with proper boundary conditions for tractions and/or displacements (Kang and Huang, 2010a).

2.2. Transversely homogeneous swelling

Now consider a hydrogel layer attached to a rigid substrate (Fig. 1). Set a Cartesian coordinate system in the dry state so that X_1 and X_3 are the in-plane coordinates and $X_2 = 0$ at the interface between the hydrogel and the substrate (Fig. 1(a)). The material parameters of the hydrogel may vary in the thickness direction, namely, $N = N(X_2)$ and $\chi = \chi(X_2)$. Immersed in a solvent, the hydrogel layer swells in the thickness direction but constrained in the in-plane directions by the substrate (assuming perfect bonding at the interface). For a transversely homogeneous swelling (Fig. 1(b)), the deformation gradient tensor is diagonal with $F_{11} = F_{33} = 1$ and $F_{22} = \mathrm{d}x_2/\mathrm{d}X_2 = \lambda_h$. By Eq. (7), the nominal stress in the swollen gel is obtained as

$$s_{22} = NkT\left[\lambda_h - \frac{1}{\lambda_h} + \frac{1}{N\Omega}\left(\log\frac{\lambda_h - 1}{\lambda_h} + \frac{1}{\lambda_h} + \frac{\chi}{\lambda_h^2} - \frac{\mu}{kT}\right)\right], \tag{11}$$

$$s_{11} = s_{33} = \frac{\lambda_h kT}{\Omega}\left(\log\frac{\lambda_h - 1}{\lambda_h} + \frac{1}{\lambda_h} + \frac{\chi}{\lambda_h^2} - \frac{\mu}{kT}\right), \tag{12}$$

and the other stress components are zero.

By the mechanical equilibrium condition in (10) along with the boundary condition at the surface, we have $s_{22} = -p$, where p is the pressure on the surface of the gel. Hence, by Eq. (11), the swelling ratio λ_h can be obtained by solving a nonlinear equation:

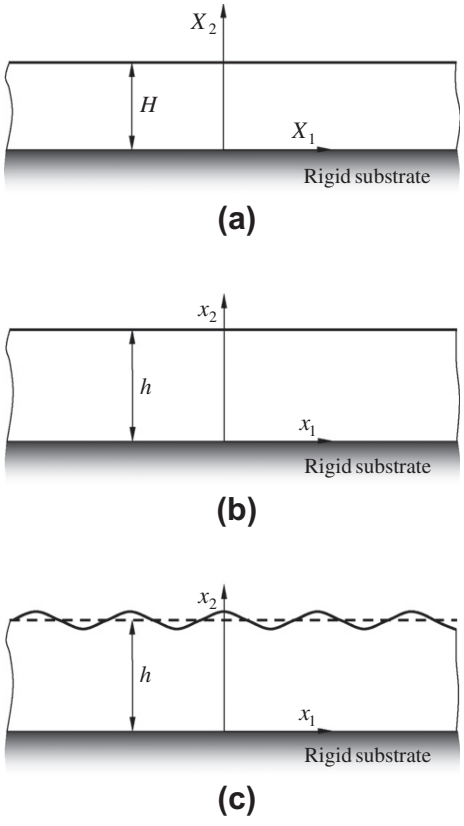

Fig. 1. Schematic of a hydrogel layer on a substrate: (a) the dry state; (b) a transversely homogeneous swollen state; (c) a perturbation to the swollen state.

$$\log\left(1 - \frac{1}{\lambda_h}\right) + \frac{1}{\lambda_h} + \frac{\chi}{\lambda_h^2} + N\Omega\left(\lambda_h - \frac{1}{\lambda_h}\right) = \frac{\mu - p\Omega}{kT}. \tag{13}$$

For a given chemical potential $\mu = \hat{\mu}$ and pressure p, the swelling ratio varies in the thickness direction, i.e., $\lambda_h = \lambda_h(X_2)$, depending on the material parameters, $N(X_2)$ and $\chi(X_2)$. The nominal concentration of the solvent vary in the thickness direction accordingly as $C(X_2) = [\lambda_h(X_2) - 1]/\Omega$. The total thickness of the hydrogel layer can be obtained by integrating the swelling ratio, i.e., $h = \int_0^H \lambda_h \mathrm{d}X_2$, where H is the thickness in the dry state.

The chemical potential of the external solvent depends on the temperature and pressure in general. Assuming an ideal gas phase ($p < p_0$) and an incompressible liquid phase ($p > p_0$), the external chemical potential is

$$\hat{\mu}(p, T) = \begin{cases} (p - p_0)\Omega, & \text{if} \quad p > p_0, \\ kT\log(p/p_0), & \text{if} \quad p < p_0, \end{cases} \tag{14}$$

where p_0 is the equilibrium vapor pressure of the solvent. Therefore, the right-hand side of Eq. (13) increases with the vapor pressure p until it reaches the equilibrium pressure ($p = p_0$). For a liquid phase solvent, the right-hand side of Eq. (13) remains a constant, $\bar{\mu}_0 = -\frac{p_0\Omega}{kT}$. For water at 25 °C, $p_0 \approx 3.2$ kPa, $\Omega \approx 3 \times 10^{-29}$ m^3, and thus $\bar{\mu}_0 \approx -2.3 \times 10^{-5}$, which is approximately taken as zero in practice.

To illustrate the effect of graded material parameters on swelling, we consider two examples, one for a hydrogel layer with linearly graded crosslink density and the other with the crosslink density varying exponentially. Since the effective number of polymer chains per unit volume is proportional to the crosslink density, we have

$$N(X_2) = N_{\text{int}} + (N_{\text{sur}} - N_{\text{int}})\frac{X_2}{H}, \tag{15}$$

or

$$N(X_2) = N_{\text{int}} + (N_{\text{sur}} - N_{\text{int}})\frac{\exp(nX_2/H) - 1}{\exp(n) - 1}, \tag{16}$$

so that $N = N_{\text{int}}$ at the hydrogel/substrate interface ($X_2 = 0$) and $N = N_{\text{sur}}$ at the surface ($X_2 = H$). The parameter n is a shape factor for the exponential function, as illustrated in Fig. 2. When $n = 0$, the exponential function in (16) reduces to the linear function in (15). The other material parameter, χ, is assumed to be a constant.

Fig. 3 shows the swelling ratio λ_h and the normalized in-plane stress $\sigma_{11}\Omega/(kT)$, in equilibrium with a liquid solvent ($\hat{\mu} = 0$) for $N_{\text{int}}\Omega = 10^{-3}$, $N_{\text{sur}}\Omega = 10^{-2}$, and $\chi = 0.4$. The nominal stress, obtained from Eq. (12), is converted to the true stress as $\sigma_{11} = s_{11}/\lambda_h$. Apparently, the transversely homogeneous swelling ratio as well as the swell-induced compressive in-plane stress varies

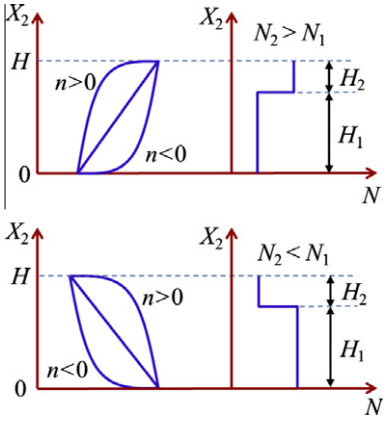

Fig. 2. Schematic illustration of the linear, exponential, and stepwise variations of the material property (N) in the thickness direction of a hydrogel layer.

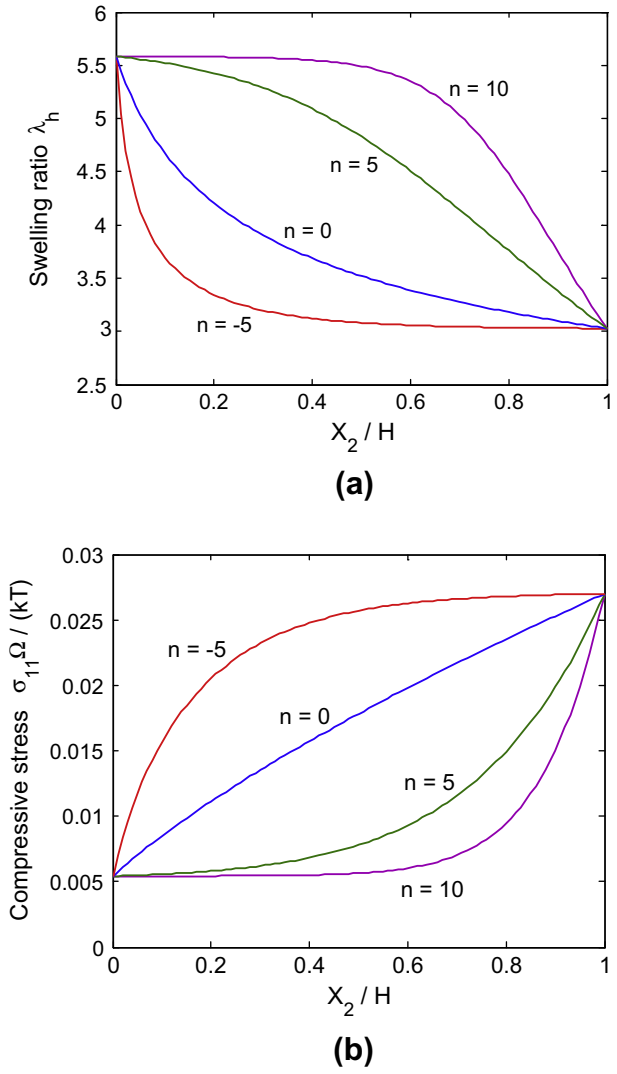

Fig. 3. (a) Swelling ratio and (b) swell-induced compressive in-plane stress for hydrogel layers with linear ($n = 0$) and exponential variations of the material parameter N in the thickness direction.

significantly from the surface to the bottom of the hydrogel layer, depending on the variation of the crosslink density in the thickness direction. The dependence is highly nonlinear, as a linear variation in the crosslink ($n = 0$) results in a nonlinear variation in the swelling ratio. Interestingly, while the swelling ratio decreases with increasing crosslink density, the magnitude of the swell-induced compressive stress increases due to increasing stiffness of the polymer network.

3. Linear perturbation analysis

The transversely homogeneous swelling may become unstable, giving rise to inhomogeneous swelling. To determine the stability, assume a small perturbation with displacements from the swollen state of a hydrogel layer in the following form (Fig. 1(c)):

$$u_1 = u_1(x_1, x_2) \quad \text{and} \quad u_2 = u_2(x_1, x_2). \tag{17}$$

The deformation gradient tensor after the perturbation becomes

$$\tilde{F} = \begin{bmatrix} 1 + \frac{\partial u_1}{\partial x_1} & \lambda_h \frac{\partial u_1}{\partial x_2} & 0 \\ \frac{\partial u_2}{\partial x_1} & \lambda_h\left(1 + \frac{\partial u_2}{\partial x_2}\right) & 0 \\ 0 & 0 & 1 \end{bmatrix}, \tag{18}$$

and the corresponding volume swelling ratio is

$$J = \det(\tilde{\mathbf{F}}) \approx \lambda_h(1 + \varepsilon), \tag{19}$$

where $\varepsilon = \frac{\partial u_1}{\partial x_1} + \frac{\partial u_2}{\partial x_2}$.

Substituting Eq. (18) into Eq. (7), the nominal stress components are obtained explicitly as follows:

$$s_{11} \approx NkT\left[(1 + \lambda_h\xi_h)\frac{\partial u_1}{\partial x_1} + \lambda_h(\xi_h - \lambda_h)\frac{\partial u_2}{\partial x_2} - \lambda_h^2 + 1\right] - p\lambda_h\left(1 + \frac{\partial u_2}{\partial x_2}\right), \tag{20}$$

$$s_{22} \approx NkT\left[(\xi_h - \lambda_h)\frac{\partial u_1}{\partial x_1} + (\xi_h + \lambda_h)\frac{\partial u_2}{\partial x_2}\right] - p\left(1 + \frac{\partial u_1}{\partial x_1}\right), \tag{21}$$

$$s_{33} \approx -NkT[\lambda_h^2(1 + \varepsilon) - \lambda_h\xi_h\varepsilon - 1] - p\lambda_h(1 + \varepsilon), \tag{22}$$

$$s_{12} \approx NkT\lambda_h\left(\frac{\partial u_1}{\partial x_2} + \frac{\partial u_2}{\partial x_1}\right) + p\frac{\partial u_2}{\partial x_1}, \tag{23}$$

$$s_{21} \approx NkT\left(\lambda_h^2\frac{\partial u_1}{\partial x_2} + \frac{\partial u_2}{\partial x_1}\right) + p\lambda_h\frac{\partial u_1}{\partial x_2}, \tag{24}$$

where $\xi_h = \frac{1}{\lambda_h} + \frac{1}{N\Omega}\left(\frac{1}{\lambda_h - 1} - \frac{1}{\lambda_h} - \frac{2\chi}{\lambda_h^2}\right)$, and $s_{23} = s_{32} = s_{13} = s_{31} = 0$. As a linear perturbation analysis, only the linear terms of the strain $\left(\frac{\partial u_i}{\partial x_j}\right)$ are retained in (19)–(24).

By the mechanical equilibrium condition in (10), we obtain a couple of linear equations in terms of the perturbation displacements:

$$(1 + \lambda_h\xi_h)\frac{\partial^2 u_1}{\partial x_1^2} + \lambda_h^2\frac{\partial^2 u_1}{\partial x_2^2} + \lambda_h\xi_h\frac{\partial^2 u_2}{\partial x_1 \partial x_2} + f_1(x_2)\left(\frac{\partial u_1}{\partial x_2} + \frac{\partial u_2}{\partial x_1}\right) = 0, \tag{25}$$

$$\frac{\partial^2 u_2}{\partial x_1^2} + \lambda_h(\xi_h + \lambda_h)\frac{\partial^2 u_2}{\partial x_2^2} + \lambda_h\xi_h\frac{\partial^2 u_1}{\partial x_1 \partial x_2} + f_2(x_2)\frac{\partial u_1}{\partial x_1} + f_3(x_2)\frac{\partial u_2}{\partial x_2} = 0, \tag{26}$$

where $f_1(x_2) = \frac{\lambda_h}{N\Omega}\frac{\mathrm{d}}{\mathrm{d}x_2}(\lambda_h N\Omega)$, $f_2(x_2) = \frac{\lambda_h}{N\Omega}\frac{\mathrm{d}}{\mathrm{d}x_2}[N\Omega(\xi_h - \lambda_h)]$, and $f_3(x_2) = \frac{\lambda_h}{N\Omega}\frac{\mathrm{d}}{\mathrm{d}x_2}[N\Omega(\xi_h + \lambda_h)]$.

Assume the perturbation displacements to be periodic in the x_1 direction, taking the form:

$$u_1 = U_1(x_2)\sin\omega x_1 \quad \text{and} \quad u_2 = U_2(x_2)\cos\omega x_1, \tag{27}$$

where ω is the wave number. Substitution of Eq. (27) into Eqs. (25) and (26) yields

$$\lambda_h^2 U_1'' + f_1 U_1' - \omega^2(1 + \lambda_h\xi_h)U_1 - \omega\lambda_h\xi_h U_2' - \omega f_1 U_2 = 0, \tag{28}$$

$$\omega\lambda_h\xi_h U_1' + \omega f_2 U_1 + \lambda_h(\xi_h + \lambda_h)U_2'' + f_3 U_2' - \omega^2 U_2 = 0, \tag{29}$$

where the single and double primes denote the first and second-order differentiations with respect to x_2. The two ordinary differential equations are to be solved along with the boundary conditions.

The lower surface of the hydrogel layer is attached to the rigid substrate with zero displacements, namely

$$U_1 = U_2 = 0, \quad \text{at} \quad x_2 = 0. \tag{30}$$

The upper surface of the hydrogel is subjected to a pressure from the external solvent. To the first order of the perturbation, the nominal traction at the surface is

$$s_{12} = p\frac{\partial u_2}{\partial x_1} \quad \text{and} \quad s_{22} = -p(1 + \frac{\partial u_1}{\partial x_1}), \ \text{at } x_2 = h. \tag{31}$$

Thus, by (21) and (23) we obtain that

$$(\xi_h - \lambda_h)\omega U_1 + (\xi_h + \lambda_h)U_2' = 0 \quad \text{and} \quad U_1' - \omega U_2 = 0, \text{ at } x_2 = h \tag{32}$$

With the boundary conditions in (30) and (32), an eigenvalue problem is established in (28) and (29) by the linear perturbation analysis. For a specific hydrogel layer with the material properties varying in the thickness direction, the solution to the eigenvalue problem depends on the chemical potential (μ). If there exists a nontrivial solution for any wave number ω, the transversely homogeneous solution becomes unstable and gives way to an inhomogeneous solution in form of Eq. (27). This condition predicts the onset of surface instability for the hydrogel layer.

We note that a similar eigenvalue problem was considered by Lee et al. (2008) for an elastic half space with graded properties. A numerical method was developed to solve the eigenvalue problem for a half space with continuously graded elastic properties. The method may be extended to solve the eigenvalue problem for the hydrogel layer with graded properties in the present study. Here, the main difference is that the linearized elastic modulus of the hydrogel layer depends on the loading parameter, i.e., the chemical potential. On the other hand, when the material properties are piecewise constant functions of x_2 (e.g., a multilayered stack), the problem can be solved analytically. In the following, we solve the eigenvalue problem analytically for hydrogel bilayers with piecewise homogeneous properties. The results are compared with two special cases, one for a homogeneous hydrogel layer as studied by Kang and Huang (2010b) and the other for the case of a thin stiff layer on a soft layer similar to thin film wrinkling (Huang, 2005; Huang et al., 2005; Cao and Hutchinson, 2012b).

4. A hydrogel bilayer model

For a homogeneous hydrogel layer, Eqs. (28) and (29) reduce to

$$\lambda_h^2 U_1'' - \omega^2(1 + \lambda_h\xi_h)U_1 - \omega\lambda_h\xi_h U_2' = 0, \tag{33}$$

$$\omega\lambda_h\xi_h U_1' + \lambda_h(\xi_h + \lambda_h)U_2'' - \omega^2 U_2 = 0, \tag{34}$$

which can be solved by

$$U_1(x_2) = A_1 e^{\omega x_2/\lambda_h} + A_2 e^{-\omega x_2/\lambda_h} + A_3 e^{\beta\omega x_2} + A_4 e^{-\beta\omega x_2}, \tag{35}$$

$$U_2(x_2) = -A_1\lambda_h e^{\omega x_2/\lambda_h} + A_2\lambda_h e^{-\omega x_2/\lambda_h} - A_3\beta e^{\beta\omega x_2} + A_4\beta e^{-\beta\omega x_2}, \tag{36}$$

where $\beta = \sqrt{(1 + \lambda_h\xi_h)/(\lambda_h^2 + \lambda_h\xi_h)}$. Applying the boundary conditions in (30) and (32), a linear system is obtained for the coefficients A_1, A_2, A_3, and A_4:

$$\mathbf{DA} = 0, \tag{37}$$

where $\mathbf{D}$ is a four by four matrix as given in Kang and Huang (2010b). The critical condition for onset of surface instability is then predicted by setting the determinant of $\mathbf{D}$ to be zero, i.e., $\det\mathbf{D} = 0$.

Next consider a hydrogel bilayer with the material properties homogeneous within each layer but different from each other (Fig. 2). The two layers are named as G1 (the bottom layer) and G2 (the top layer), with the material properties N_i and χ_i for $i = 1$ and 2, respectively. In the dry state, the thicknesses of the two layers are, respectively, H_1 and H_2, with the total thickness $H = H_1 + H_2$. When immersed in a solvent of a constant chemical potential, the two layers swell in the thickness direction, and their thicknesses become h_1 and h_2, with the total thickness $h = h_1 + h_2$. By Eq. (13), the transversely homogeneous swelling ratio of each layer can be obtained as a function of the chemical potential, i.e., $h_i/H_i = \lambda_{hi}(\mu)$, and the average swelling ratio of the bilayer is then

$$\lambda_h = h/H = \lambda_{h1}(1 - \eta) + \lambda_{h2}\eta, \tag{38}$$

where $\eta = H_2/H$ is the volume fraction of the top layer in the dry state.

Fig. 4(a) plots the swelling ratios λ_{hi} for a bilayer with $N_i\Omega = 10^{-3}$ and 10^{-2} whereas $\chi_1 = \chi_2 = 0.4$. Correspondingly, the compressive in-plane stresses induced by swelling are plotted in Fig. 4(b). With a higher crosslink density in the top layer ($N_2 > N_1$), the swelling ratio is lower but the induced compressive stress is higher due to the higher elastic stiffness. It is noted that the swelling ratios of the two layers are nearly identical for a relatively low chemical potential (e.g., $\mu < -0.1$), while the swell-induced compressive stresses differ considerably.

For the linear perturbation analysis, the perturbation displacements in each layer are: $u_1^{(i)} = U_1^{(i)}(x_2)\sin\omega x_1$ and $u_2^{(i)} = U_2^{(i)}(x_2)\cos\omega x_1$ (i = 1 and 2). For each homogeneous layer, the perturbation displacements are obtained in the same form as the homogeneous case:

$$U_1^{(i)} = A_1^{(i)} e^{\omega x_2/\lambda_{hi}} + A_2^{(i)} e^{-\omega x_2/\lambda_{hi}} + A_3^{(i)} e^{\beta_i\omega x_2} + A_4^{(i)} e^{-\beta_i\omega x_2}, \tag{39}$$

$$U_2^{(i)} = -A_1^{(i)}\lambda_{hi} e^{\omega x_2/\lambda_{hi}} + A_2^{(i)}\lambda_{hi} e^{-\omega x_2/\lambda_{hi}} - A_3^{(i)}\beta_i e^{\beta_i\omega x_2} + A_4^{(i)}\beta_i e^{-\beta_i\omega x_2}, \tag{40}$$

where $\beta_i = \sqrt{(1 + \lambda_{hi}\xi_{hi})/(\lambda_{hi}^2 + \lambda_{hi}\xi_{hi})}$.

For the bilayer, in addition to the boundary conditions in (30) and (32), the perturbation displacements and the associated tractions ($T_i = s_{iK}N_K$) must be continuous across the interface at $x_2 = h_1$, namely

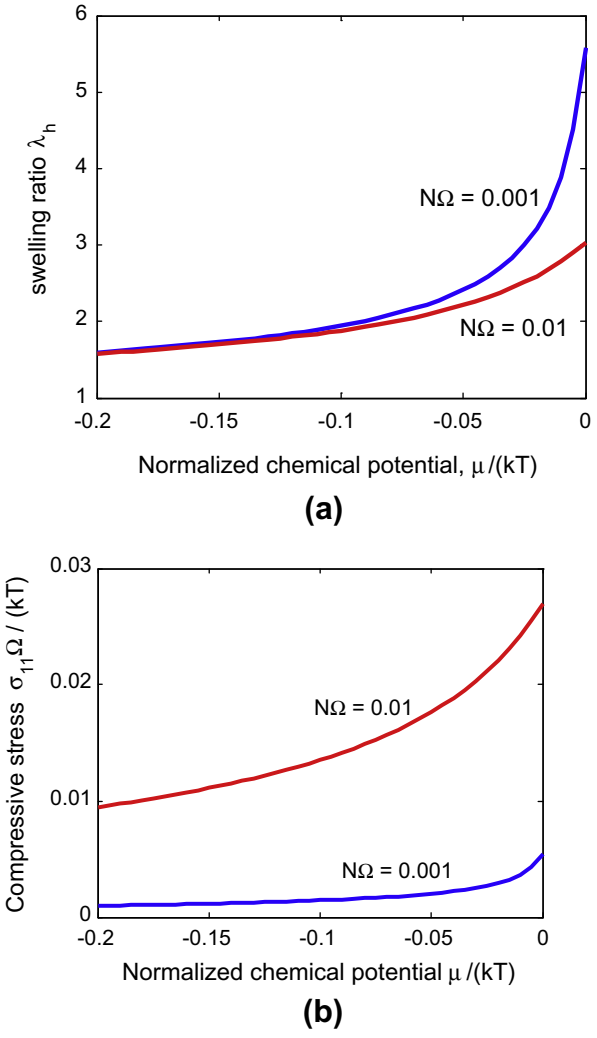

Fig. 4. (a) Swelling ratios and (b) magnitudes of the in-plane stresses with respect to the normalized chemical potential for a hydrogel bilayer with $N\Omega = 10^{-3}$ and 10^{-2}.

$$U_1^{(1)}(h_1) = U_1^{(2)}(h_1) \quad \text{and} \quad U_2^{(1)}(h_1) = U_2^{(2)}(h_1), \tag{41}$$

$$s_{12}^{(1)}(h_1) = s_{12}^{(2)}(h_1) \quad \text{and} \quad s_{22}^{(1)}(h_1) = s_{22}^{(2)}(h_1). \tag{42}$$

Therefore, the eight coefficients $A_m^{(1)}$ and $A_m^{(2)}$ (m = 1–4) must satisfy the eight Eqs. in (30), (32), (41) and (42), which can be written in a matrix form:

$$\mathbf{DA} = 0, \tag{43}$$

where $\mathbf{A} = \left[A_1^{(1)} A_2^{(1)} A_3^{(1)} A_4^{(1)} A_1^{(2)} A_2^{(2)} A_3^{(2)} A_4^{(2)}\right]^T$ and $\mathbf{D}$ is a 8×8 matrix with the following nonzero elements:

$$D_{11} = D_{12} = D_{13} = D_{14} = 1,$$
$$D_{21} = -D_{22} = \lambda_{h1}, \quad D_{23} = -D_{24} = \beta_1,$$
$$D_{31} = e^{\omega h_1/\lambda_{h1}}, \quad D_{32} = e^{-\omega h_1/\lambda_{h1}}, \quad D_{33} = e^{\beta_1 \omega h_1}, \quad D_{34} = e^{-\beta_1 \omega h_1},$$
$$D_{35} = -e^{\omega h_1/\lambda_{h2}}, \quad D_{36} = -e^{-\omega h_1/\lambda_{h2}}, \quad D_{37} = -e^{\beta_2 \omega h_1}, \quad D_{38} = -e^{-\beta_2 \omega h_1},$$
$$D_{41} = \lambda_{h1} e^{\omega h_1/\lambda_{h1}}, \quad D_{42} = -\lambda_{h1} e^{-\omega h_1/\lambda_{h1}}, \quad D_{43} = \beta_1 e^{\beta_1 \omega h_1}, \quad D_{44} = -\beta_1 e^{-\beta_1 \omega h_1},$$
$$D_{45} = -\lambda_{h2} e^{\omega h_1/\lambda_{h2}}, \quad D_{46} = \lambda_{h2} e^{-\omega h_1/\lambda_{h2}}, \quad D_{47} = -\beta_2 e^{\beta_2 \omega h_1}, \quad D_{48} = \beta_2 e^{-\beta_2 \omega h_1},$$
$$D_{51} = 2N_1\Omega\lambda_{h1} e^{\omega h_1/\lambda_{h1}}, \quad D_{52} = 2N_1\Omega\lambda_{h1} e^{-\omega h_1/\lambda_{h1}},$$
$$D_{53} = N_1\Omega(\lambda_{h1} + 1/\lambda_{h1}) e^{\beta_1 \omega h_1}, \quad D_{54} = N_1\Omega(\lambda_{h1} + 1/\lambda_{h1}) e^{-\beta_1 \omega h_1},$$
$$D_{55} = -2N_2\Omega\lambda_{h2} e^{\omega h_1/\lambda_{h2}}, \quad D_{56} = -2N_2\Omega\lambda_{h2} e^{-\omega h_1/\lambda_{h2}},$$
$$D_{57} = -N_2\Omega(\lambda_{h2} + 1/\lambda_{h2}) e^{\beta_2 \omega h_1}, \quad D_{58} = -N_2\Omega(\lambda_{h2} + 1/\lambda_{h2}) e^{-\beta_2 \omega h_1},$$
$$D_{61} = N_1\Omega(\lambda_{h1}^2 + 1) e^{\omega h_1/\lambda_{h1}}, \quad D_{62} = -N_1\Omega(\lambda_{h1}^2 + 1) e^{-\omega h_1/\lambda_{h1}},$$
$$D_{63} = 2N_1\Omega\lambda_{h1}\beta_1 e^{\beta_1 \omega h_1}, \quad D_{64} = -2N_1\Omega\lambda_{h1}\beta_1 e^{-\beta_1 \omega h_1},$$
$$D_{65} = -N_2\Omega(\lambda_{h2}^2 + 1) e^{\omega h_1/\lambda_{h2}}, \quad D_{66} = N_2\Omega(\lambda_{h2}^2 + 1) e^{-\omega h_1/\lambda_{h2}},$$
$$D_{67} = -2N_2\Omega\lambda_{h2}\beta_2 e^{\beta_2 \omega h_1}, \quad D_{68} = 2N_2\Omega\lambda_{h2}\beta_2 e^{-\beta_2 \omega h_1},$$
$$D_{75} = 2\lambda_{h2} e^{\omega h/\lambda_{h2}}, \quad D_{76} = 2\lambda_{h2} e^{-\omega h/\lambda_{h2}},$$
$$D_{77} = (\lambda_{h2} + 1/\lambda_{h2}) e^{\beta_2 \omega h}, \quad D_{78} = (\lambda_{h2} + 1/\lambda_{h2}) e^{-\beta_2 \omega h},$$
$$D_{85} = (\lambda_{h2} + 1/\lambda_{h2}) e^{\omega h/\lambda_{h2}}, \quad D_{86} = -(\lambda_{h2} + 1/\lambda_{h2}) e^{-\omega h/\lambda_{h2}},$$
$$D_{87} = 2\beta_2 e^{\beta_2 \omega h}, \quad D_{88} = -2\beta_2 e^{-\beta_2 \omega h}.$$

The critical condition for onset of the surface instability in the hydrogel bilayer is then obtained by setting the determinant of the matrix $\mathbf{D}$ equal to zero, namely

$$\det(\mathbf{D}) = f(\omega H, \mu; N_1\Omega, N_2\Omega, \chi_1, \chi_2, \eta) = 0. \tag{44}$$

For each normalized wave number (ωH), we solve (44) to find the critical chemical potential μ_c, which depends on the material properties of the bilayer ($N_1\Omega$, $N_2\Omega$, χ_1, and χ_2) as well as the volume fraction η. The swelling ratio of each layer at the critical chemical potential, $\lambda_{hi}(\mu_c)$, is then obtained from Eq. (13). Subsequently, the average critical swelling ratio for the bilayer λ_c is calculated following Eq. (38).

5. Results and discussion

In this section, we present the quantitative results from the stability analysis of hydrogel bilayers and discuss the effects of material properties. Fig. 5(a) plots the critical chemical potental as a function of the perturbation wave number for two bilayers (A and B), in comparison with a homogeneous layer. The corresponding critical swelling ratios are plotted in Fig. 5(b). For the homogeneous layer ($N\Omega$ = 0.001 and χ = 0.4), both the critical chemical potential and the critical swelling ratio decreases monotonically with increasing wave number. The long-wave modes (small wave numbers) of perturbation are stablized by the rigid substrate, while the short-wave modes ($\omega \to \infty$) are independent of the substrate. Consequently, the onset of surface stability is determined at the short-wave limit (Kang and Huang, 2010b), with no characteristic length scale. For the bilayers, however, the critical chemical potential varies with the perturbation wave number non-monotonically.

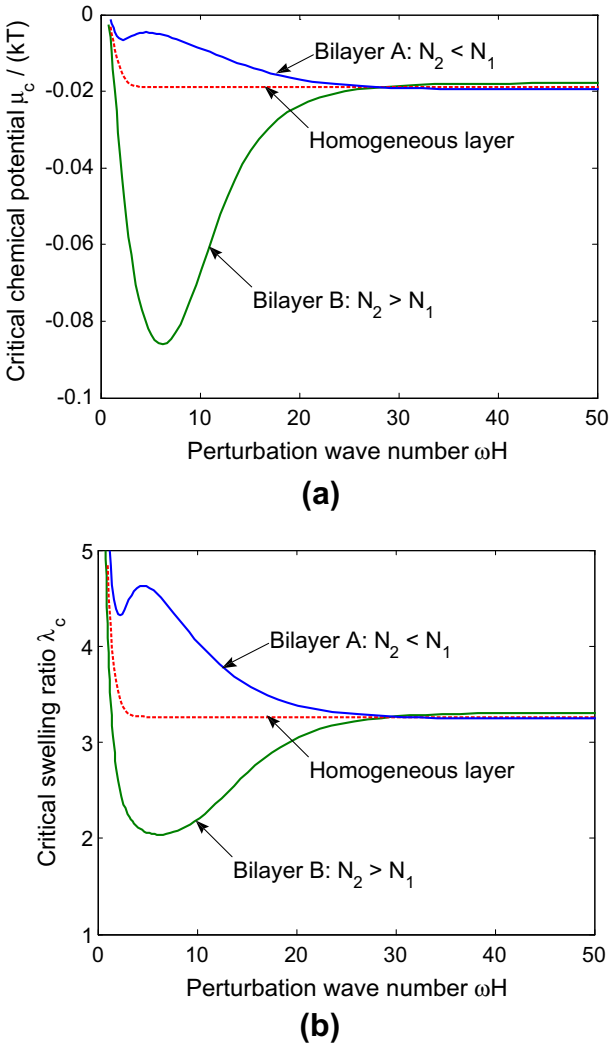

Fig. 5. (a) Critical chemical potential and (b) the corresponding swelling ratio versus the perturbation wave number for two hydrogel bilayers (A: $N_2\Omega = 4 \times 10^{-4}$; B: $N_2\Omega = 2 \times 10^{-3}$), both with $N_1\Omega = 10^{-3}$ and $\eta = 0.1$, in comparison with a homogeneous hydrogel layer ($N\Omega = 10^{-3}$).

If the top layer is softer than the underlayer ($N_2 < N_1$), the critical chemical potential has a local minimum μ_c^*, corresponding to a long-wavelength mode ($\omega = \omega^*$). The local minimum μ_c^* however is greater than the critical chemical potential at the short-wave limit ($\omega \to \infty$), i.e., $\mu_c^* > \mu_c^\infty$. Therefore, the onset of surface instability for such a bilayer (*soft-on-hard*) is expected to be determined by the short-wave limit. The presence of a local minimum suggests a possible metastable state of surface instability for the soft-on-hard bilayer. On the other hand, if the top layer is stiffer than the underlayer ($N_2 > N_1$), the minimum critical chemical potential occurs at a long-wave mode and is lower than the short-wave limit, i.e., $\mu_c^* < \mu_c^\infty$. Consequently, the critical condition for onset of surface instability for such a bilayer (*hard-on-soft*) is determined by a critical long-wave mode, with a characteristic length ($L^* = 2\pi/\omega^*$). In this case, the critical chemical potential as well as the corresponding critical swelling ratio can be considerably lower than that for a homogeneous layer. Therefore, the two types of hydrogel bilayers (soft-on-hard vs hard-on-soft) exhibit distinct behavior at the onset of surface instability: for the soft-on-hard bilayer, with no characteristic length, surface wrinkling is highly unstable and is likely to collapse into creases; for the hard-on-soft bilayer, surface wrinkling is stable with a finite wavelength.

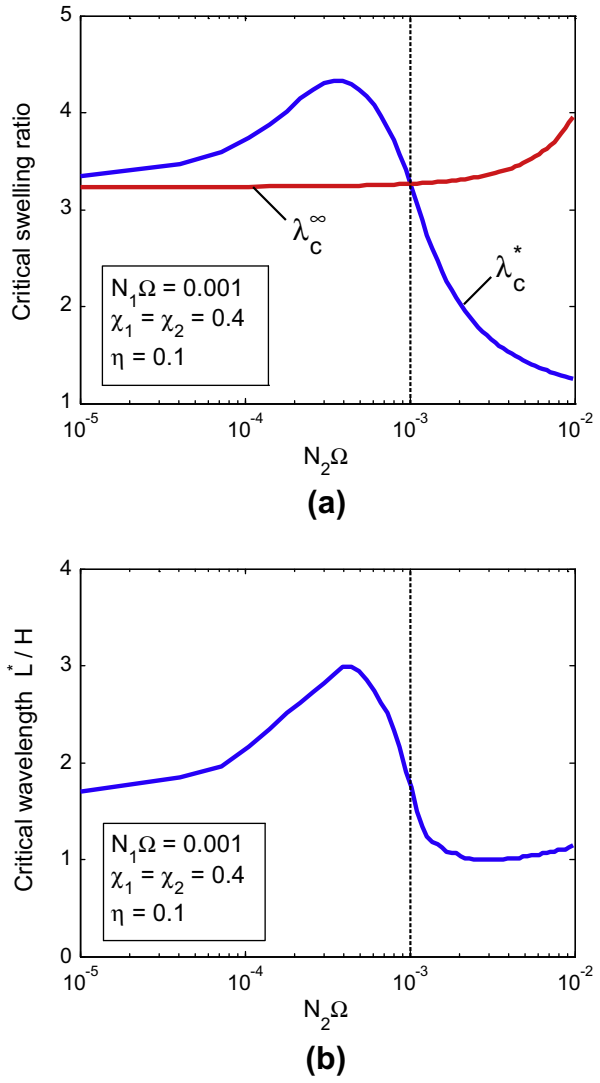

Fig. 6. (a) The critical swelling ratios for the long-wave mode and the short-wave limit, and (b) the critical wavelength corresponding to the long-wave mode, for hydrogel bilayers with $N_2\Omega$ ranging from 10^{-5} to 10^{-2}.

Fig. 6(a) plots the critical swelling ratios for the short-wave limit and the long-wave mode for hydrogel bilayers as $N_2\Omega$ changes in the upper layer while $N_1\Omega = 0.001$ is fixed for the underlayer. It can be shown that the critical chemical potential at the short-wave limit (μ_c^∞) depends on the upper layer only, which is identical to that for a homogeneous layer with the same properties and can be written in an implicit form as (Kang and Huang, 2010b)

$$\left(\lambda_{h2} + \frac{1}{\lambda_{h2}}\right)^2 - 4\lambda_{h2}\beta_2 = 0. \tag{45}$$

As $N_2\Omega$ increases, the critical chemical potential (μ_c^∞) increases. Thus, the critical chemical potential for a soft-on-hard bilayer ($N_2 < N_1$) is slightly lower than that for a homogeneous layer with the same property as the underlayer, while the critical chemical potential at the short-wave limit for a hard-on-soft bilayer ($N_2 > N_1$) is higher, as shown in Fig. 5(a). On the other hand, as $N_2\Omega$ increases, the critical swelling ratio for the upper layer (λ_{h2}) decreases (Kang and Huang, 2010b), but the swelling ratio of the underlayer (λ_{h1}) increases with the chemical potential. Since the critical swelling ratio for a bilayer is defined as the average of the swelling ratios in the two layers at the critical chemical potential, it may increase or decrease, depending on the volume ratio η by Eq. (38). With $\eta = 0.1$ in Fig. 6(a), the critical swelling ratio at the short-wave limit (λ_c^∞) increases with increasing $N_2\Omega$.

As shown in Fig. 6(a), the critical swelling ratio for the long-wave mode (λ_c^*) is greater than λ_c^∞ for a soft-on-hard bilayer ($N_2\Omega < N_1\Omega$), but is lower for a hard-on-soft bilayer ($N_2\Omega > N_1\Omega$). In the latter case, the critical swelling ratio λ_c^* decreases as $N_2\Omega$ increases, which can be significantly lower than the critical swelling ratio for a homogeneous layer. Previously, Kang and Huang (2010b) predicted the critical swelling ratio for a homogeneous hydrogel layer to be in the range of 2.5–3.4 for onset of wrinkling instability, and Weiss et al. (Submitted for publication) predicted the critical swelling ratio to be much lower (~2.0) for onset of creasing instability. In experiments, for hydrogel films with depth-wise crosslink gradients, Guvendiren et al. (2010a,b) reported the critical swelling ratio to be 1.12 for wrinkling and in the range of 1.3–2.0 for creasing, both considerably lower than the counterparts for a homogeneous layer. In their experiments, the top layer had a lower crosslink density, which gradually increased with the depth, similar to the soft-on-hard bilayer model. However, the reported low critical swelling ratios for wrinkling and creasing seem to be more consistent with the hard-on-soft bilayer model in the present study. It is noted that others have reported formation of a hard skin layer on the surface of a polymer film exposed to UV curing (Godinho et al., 2006). With limited information from experiments, a direct comparison between the theoretical prediction and the experiments is not possible at the moment.

Fig. 6(b) plots the wavelength of the critical long-wave mode ($L^* = 2\pi/\omega^*$), normalized by the bilayer thickness ($H = H_1 + H_2$). When $N_2\Omega > N_1\Omega$, the critical wavelength first decreases and then increases slowly with increasing $N_2\Omega$. By a dimensional consideration, the normalized critical wavelength is a function of the dimensionless parameters including the volume fraction η, $N_1\Omega$, $N_2\Omega$, χ_1 and χ_2. Numerically it scales linearly with the thickness H, with the proportionality in the order of unity ($L^*/H \sim 1$). Incidentally, previous studies have predicted critical wavelengths in the order of the layer thickness by considering the effect of surface tension (Kang and Huang, 2010c; Ben Amar and Ciarletta, 2010; Dervaux and Ben Amar, 2011). Experimental observations have also reported characteristic length scales of the surface instability patterns proportional to the initial layer thickness (Trujillo et al., 2008; Guvendiren et al., 2009).

The bilayer model allows consideration of two limiting cases and the transition in between. When the volume fraction η approaches 1, the bilayer model recovers the case of a homogeneous layer. On the other hand, when η approaches 0 (but not exactly 0), the top layer can be treated as a thin film lying on a thick substrate. The critical swelling ratio as a function of the volume fraction (η) is shown in Fig. 7. For a soft-on-hard bilayer (Fig. 7(a)), the critical swelling ratio for the short-wave limit (λ_c^∞) increases slightly as η increases. Meanwhile, the critical swelling ratio for the long-wave mode (λ_c^*) increases abruptly for $\eta < 0.13$, beyond which the local minimum as shown in Fig. 5 degenerates into an inflection point and hence no critical mode is predicted other than the short-wave limit. We note that, since the critical chemical potential at the short-wave limit (μ_c^∞) as predicted by Eq. (45) is independent of the volume fraction, the corresponding critical swelling ratio (λ_c^∞) varies linearly with respect to η between $\lambda_{h1}(\mu_c^\infty)$ and $\lambda_{h2}(\mu_c^\infty)$. For a hard-on-soft bilayer (Fig. 7(b)), the critical swelling ratio for the short-wave limit (λ_c^∞) decreases slightly as η increases, which is expected as $\lambda_{h2}(\mu_c^\infty) < \lambda_{h1}(\mu_c^\infty)$ for $N_2\Omega > N_1\Omega$. In this case, the critical long-wave mode persists over the entire range of η, and the critical swelling ratio λ_c^* is lower than λ_c^∞. As η approaches 1, the two critical swelling ratios converge at the limit of a homogeneous layer. The difference between the two

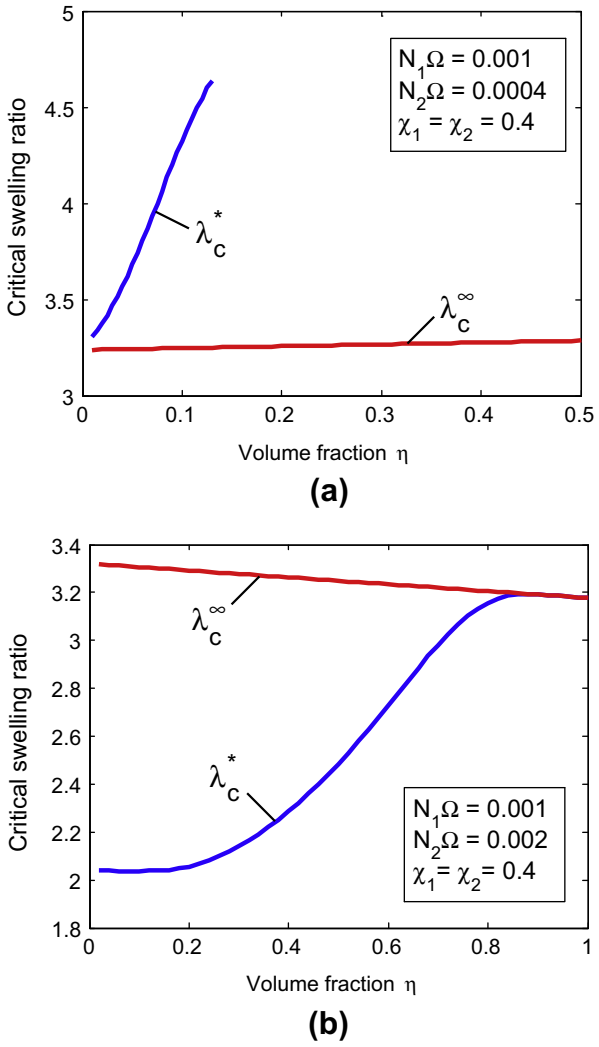

Fig. 7. The critical swelling ratios versus the volume fraction of the upper layer for: (a) soft-on-hard hydrogel bilayers, and (b) hard-on-soft hydrogel bilayers.

critical chemical potentials is less than 10^{-6} (after normalization) when $\eta > 0.92$. At the other end, when η approaches 0, the critical swelling ratio (λ_c^*) approaches a considerably lower value. With a thin, stiff upper layer on a thick, soft underlayer, this is taken as the thin-film limit, for which similar wrinkling instability has been studied extensively (Chen and Hutchinson, 2004; Huang, 2005; Huang et al., 2005; Lee et al., 2008; Audoly and Boudaoud, 2008; Sultan and Boudaoud, 2008; Cao and Hutchinson, 2012b). Between the thin-film limit ($\eta \to 0$) and the homogeneous limit ($\eta \to 1$), the critical instability mode for a hard-on-soft bilayer undergoes a smooth transition from the long-wave mode to the short-wave mode.

For the thin-film limit, an approximate critical condition can be developed based on previous studies on thin film wrinkling (Huang, 2005; Huang et al., 2005). Here, the upper layer is treated as an elastic thin film subject to a compressive in-plane stress due to swelling. By Eqs. (12) and (13), the swell-induced compressive stress in the upper layer is

$$\sigma = -N_2 kT\left(\lambda_{h2} - \frac{1}{\lambda_{h2}}\right). \tag{46}$$

Taking the lower layer as a linearly elastic substrate of infinite thickness, the critical stress for wrinkling is

$$\sigma_c = -\left[\frac{9G_1^2 G_2}{8(1-\nu_1)^2(1-\nu_2)}\right]^{1/3}, \tag{47}$$

where G_i and ν_i are the shear modulus and Poisson's ratio of the two layers ($i = 1$ and 2). In general, both the shear modulus and the Poisson's ratio of a swollen hydrogel depend on the chemical potential or the swelling ratio (Bouklas and Huang, 2012). Moreover, the anisotropic swelling due to substrate constraint would lead to anisotropic elastic properties for the hydrogel layers. As an approximation, we take $G_i \approx N_i kT$ and $\nu_i \approx 0.5$. Thus the critical condition in (47) becomes approximately

$$\left(\lambda_{h2} - \frac{1}{\lambda_{h2}}\right)^3 = \left(\frac{3N_1}{N_2}\right)^2, \tag{48}$$

which predicts the critical swelling ratio for the upper layer as a function of the ratio N_1/N_2. The corresponding critical chemical potential can then be obtained from Eq. (13), with which the critical swelling ratio for the underlayer (λ_{h1}) can be determined. With $\eta \to 0$, the critical swelling ratio of the bilayer is approximately that of the underlayer ($\lambda_h \approx \lambda_{h1}$). Moreover, based on the thin film wrinkling analysis (Huang, 2005; Huang et al., 2005), the critical wrinkle wavelength for the hydrogel bilayer is predicted as

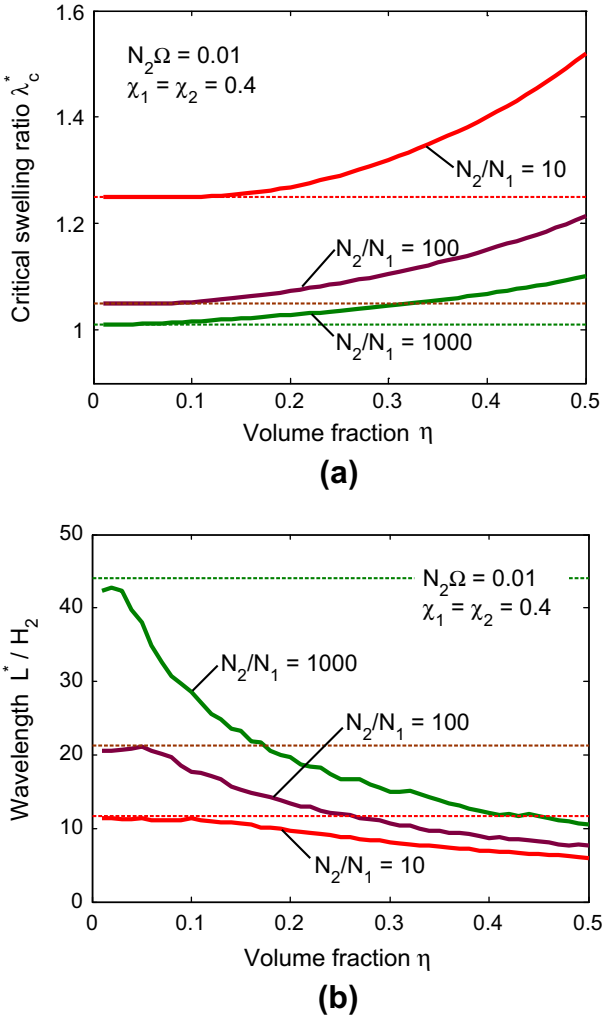

Fig. 8. (a) Critical swelling ratio and (b) the corresponding perturbation wavelength, versus the volume fraction for hard-on-soft hydrogel bilayers ($N_2 > N_1$). The horizontal dashed lines in both figures are the approximate solutions at the thin-film limit ($\eta \to 0$).

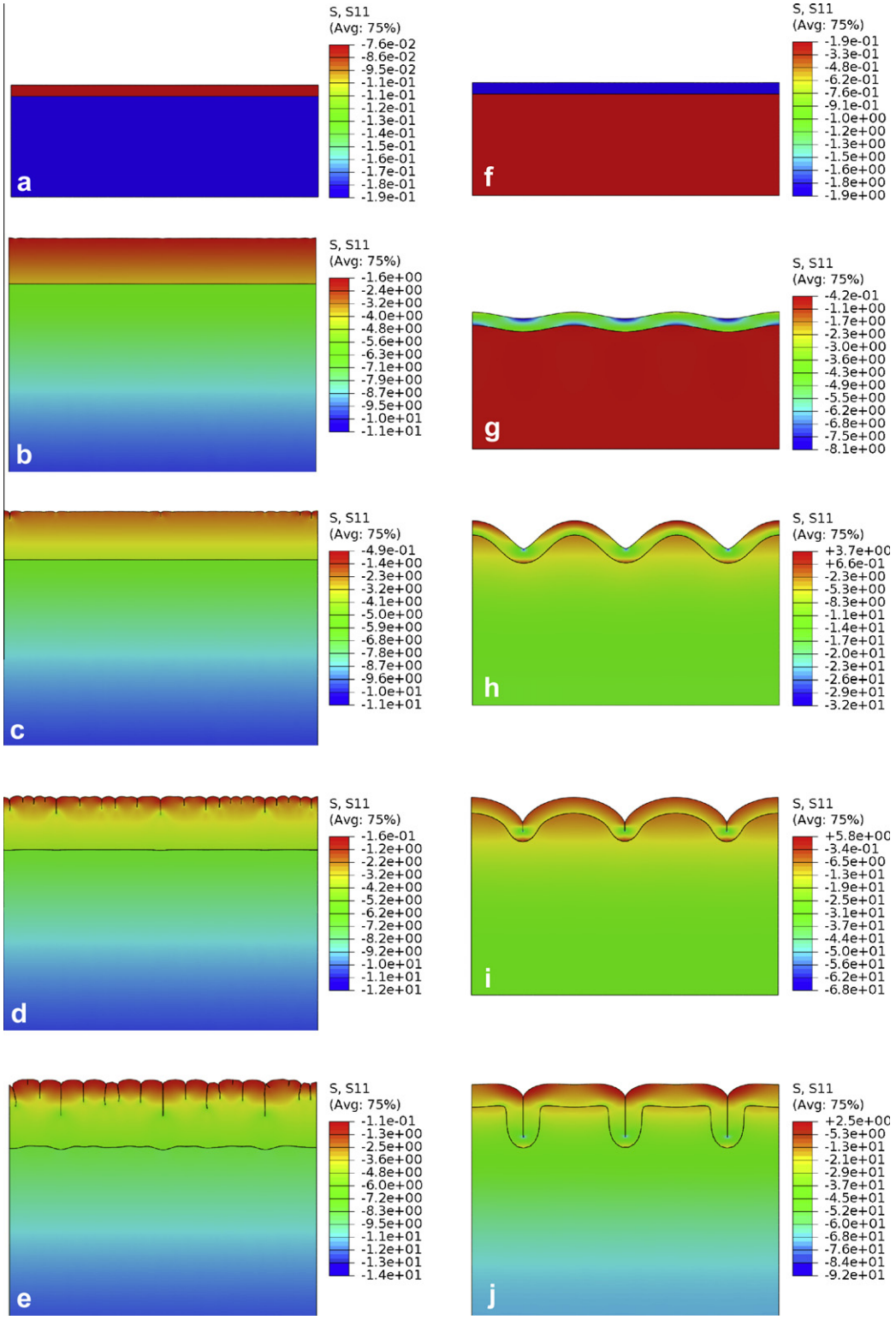

Fig. 9. Numerical simulations of swell-induced surface instability. (a–e): $\mu/kT = -1.158$, -0.0068, -0.006, -0.004 and 0 for a soft-on-hard bilayer ($N_1\Omega = 10^{-3}$ and $N_2\Omega = 4 \times 10^{-4}$); (f–j): $\mu/kT = -1.158$, -0.437, -0.1513, -0.095 and 0 for a hard-on-soft bilayer ($N_1\Omega = 10^{-3}$ and $N_2\Omega = 10^{-2}$).

$$L^* = 2\pi h_2 \left[\frac{G_2(1-\nu_1)}{3G_1(1-\nu_2)}\right]^{1/3} \approx 2\pi H_2 \lambda_{h2} \left(\frac{N_2}{3N_1}\right)^{1/3}. \tag{49}$$

Fig. 8 plots the critical swelling ratio (λ_c^*) and the corresponding wavelength (L^*/H_2) with respect to the volume fraction η for different N_2/N_1ratios, comparing the thin-film approximation (dashed lines) to the exact solution by the linear perturbation analysis (solid lines). As the ratio N_2/N_1 increases, λ_c^* decreases rapidly and L^*/H_2 increases. As $\eta \to 0$, the exact solution approaches the thin-film limit, in close agreement with the approximate solutions for both the critical swelling ratio and the wrinkle wavelength. The agreement however becomes less satisfactory when $N_2/N_1 < 10$, since

the assumption of the linear elastic properties for the swollen hydrogel layers is limited to relatively small swelling ratios (Bouklas and Huang, 2012).

Finally we present two numerical examples to highlight the distinct surface instability behaviors for the soft-on-hard and hard-on-soft hydrogel bilayers. A nonlinear finite element method developed previously (Kang and Huang, 2010a) is used to simulate swell-induced deformation and evolution of surface instability of the hydrogel bilayers, as shown in Fig. 9. The numerical procedure is similar to that for a homogeneous layer in Kang and Huang (2010b). The two models are identical in geometry, mesh, initial surface perturbation, and boundary conditions. The common material properties are: $N_1\Omega = 10^{-3}$ and $\chi_1 = \chi_2 = 0.4$. The soft-on-hard bilayer, with $N_2\Omega = 4 \times 10^{-4}$, develops multiple surface creases without appreciable wrinkling (Fig. 9(a)–(e)), similar to that of a homogeneous layer (Kang and Huang, 2010b). For the hard-on-soft bilayer, with $N_2\Omega = 10^{-2}$, the behavior is drastically different: the wrinkles grow significantly before creases form (Fig. 9(f)–(j)). The critical chemical potential or the critical swelling ratio for the onset of surface wrinkling in the hard-on-soft bilayer is considerably lower than that for surface creasing in the soft-on-hard bilayer. While the wrinkles eventually evolve to form creases on the surface of the hard-on-soft bilayer, the locations of surface creases are well defined at the bottom of the wrinkle troughs. As noted in previous studies (Hong et al., 2009b; Weiss, Submitted for publication), the critical condition for surface creasing is autonomous. In other words, the critical chemical potential for surface creasing in the bilayer should be identical to that for a homogeneous layer with the same material properties as the upper layer. This is indeed the case for the soft-on-hard bilayer, where formation of surface creases precedes wrinkling (Fig. 9(a)–(e)). For the hard-on-soft bilayer, however, the critical chemical potential for wrinkling is much lower than that for creasing. In this case, formation of surface wrinkles precedes creasing (Fig. 9(f)–(j)). More detailed discussions of the numerical simulations and post-instability evolution of the surface patterns will be presented elsewhere.

6. Summary

This paper presents a theoretical stability analysis for swelling of hydrogel layers with material properties varying in the thickness direction. As a specialization of the general procedure, hydrogel bilayers with different combinations of the material properties are examined in details. The results suggest that both the critical condition and the instability mode depend sensitively on the variation of the material properties in the thickness direction of the hydrogel layer. For a soft-on-hard bilayer, the onset of surface instability is determined by the short-wave limit, with no characteristic length. In contrast, for a hard-on-soft bilayer, a long-wave mode emerges as the critical mode at the onset of surface instability, with a finite wavelength, similar to wrinkling of an elastic thin film on a compliant substrate; moreover, the critical swelling ratio can be much lower than that for a homogeneous hydrogel layer. A smooth transition between two limiting cases (homogeneous and thin-film limits) is predicted as the volume fraction of the top layer changes. At the thin-film limit, the predicted critical condition and the wavelength agree closely with an approximate solution based on the previous studies of thin-film wrinkling.

Acknowledgments

The authors gratefully acknowledge funding of this work by National Science Foundation through Grant No. 1200161. ZW was supported by Hefei University of Technology (China) as a visiting scholar at The University of Texas at Austin.

References

Audoly, B., Boudaoud, A., 2008. Buckling of a stiff film bound to a compliant substrate – Part I: Formulation, linear stability of cylindrical patterns, secondary bifurcations. J. Mech. Phys. Solids 56, 2401–2421.
Ben Amar, M., Ciarletta, P., 2010. Swelling instability of surface-attached gels as a model of soft tissue growth under geometric constraints. J. Mech. Phys. Solids 58, 935–954.
Biot, M.A., 1963. Surface instability of rubber in compression. Appl. Sci. Res. A 12, 168–182.
Bouklas, N., Huang, R., 2012. Swelling kinetics of polymer gels: comparison of linear and nonlinear theories. Soft Matter 8, 8194–8203.
Cao, Y., Hutchinson, J.W., 2012a. From wrinkles to creases in elastomers: the instability and imperfection-sensitivity of wrinkling. Proc. Royal Soc. A 468, 94–115.
Cao, Y., Hutchinson, J.W., 2012b. Wrinkling phenomena in Neo-Hookean film/substrate bilayers. J. Appl. Mech. 79, 031019.
Cao, Y.-P., Li, B., Feng, X.-Q., 2012. Surface wrinkling and folding of core-shell soft cylinders. Soft Matter 8, 556–562.
Chen, X., Hutchinson, J.W., 2004. Herringbone buckling patterns of compressed thin films on compliant substrates. J. Appl. Mech. 71, 597–603.
Dervaux, J., Ben Amar, M., 2011. Buckling condensation in constrained growth. J. Mech. Phys. Solids 59, 538–560.
Dervaux, J., Couder, Y., Guedeau-Boudeville, M.-A., Ben Amar, M., 2011. Shape transition in artificial tumors: from smooth buckles to singular creases. Phys. Rev. Lett. 107, 018103.
Flory, P.J., 1942. Thermodynamics of high polymer solutions. J. Chem. Phys. 10, 51–61.
Flory, P.J., Rehner Jr., J., 1943a. Statistical mechanics of cross-linked polymer networks. I. Rubberlike elasticity. J. Chem. Phys. 11, 512–520.
Flory, P.J., Rehner Jr., J., 1943b. Statistical mechanics of cross-linked polymer networks. II. Swelling. J. Chem. Phys. 11, 521–526.
Gent, A.N., Cho, I.S., 1999. Surface instabilities in compressed or bent rubber blocks. Rubber Chem. Technol. 72, 253–262.
Godinho, M.H., Trindade, A.C., Figueirinhas, J.L., Melo, L.V., Brogueira, P., Deus, A.M., et al., 2006. Tuneable micro- and nano-periodic structures in a free-standing flexible urethane/urea elastomer film. Eur. Phys. J. E 21, 319–330.
Guvendiren, M., Yang, S., Burdick, J.A., 2009. Swelling-induced surface patterns in hydrogels with gradient crosslinking density. Adv. Funct. Mater. 19, 3038–3045.
Guvendiren, M., Burdick, J.A., Yang, S., 2010a. Kinetic study of swelling-induced surface pattern formation and ordering in hydrogel films with depth-wise crosslinking gradients. Soft Matter 6, 2044–2049.
Guvendiren, M., Burdick, J.A., Yang, S., 2010b. Solvent induced transition from wrinkles to creases in thin film gels with depth-wise crosslinking gradients. Soft Matter 6, 5795–5801.
Hohlfeld, E., Mahadevan, L., 2011. Unfolding the sulcus. Phys. Rev. Lett. 106, 105702.
Hong, W., Liu, Z., Suo, Z., 2009a. Inhomogeneous swelling of a gel in equilibrium with a solvent and mechanical load. Int. J. Solids Struct. 46, 3282–3289.
Hong, W., Zhao, X., Suo, Z., 2009b. Formation of creases on the surfaces of elastomers and gels. Appl. Phys. Lett. 95, 111901.
Hong, W., Zhao, X., Zhou, J., Suo, Z., 2008. A theory of coupled diffusion and large deformation in polymeric gels. J. Mech. Phys. Solids 56, 1779–1793.
Huang, R., 2005. Kinetic wrinkling of an elastic film on a viscoelastic substrate. J. Mech. Phys. Solids 53, 63–89.
Huang, Z.Y., Hong, W., Suo, Z., 2005. Nonlinear analyses of wrinkles in a film bonded to a compliant substrate. J. Mech. Phys. Solids 53, 2101–2118.
Huggins, M.L., 1941. Solutions of long chain compounds. J. Chem. Phys. 9, 440.
Kang, M.K., Huang, R., 2010a. A variational approach and finite element implementation for swelling of polymeric hydrogels under geometric constraints. J. Appl. Mech. 77, 061004.
Kang, M.K., Huang, R., 2010b. Swell-induced surface instability of confined hydrogel layers on substrates. J. Mech. Phys. Solids 58, 1582–1598.
Kang, M.K., Huang, R., 2010c. Effect of surface tension on swell-induced surface instability of substrate-confined hydrogel layers. Soft Matter 6, 5736–5742.
Lee, D., Triantafyllidis, N., Barber, J.R., Thouless, M.D., 2008. Surface instability of an elastic half space with material properties varying with depth. J. Mech. Phys. Solids 56, 858–868.
Onuki, A., 1989. Theory of pattern formation in gels: surface folding in highly compressible elastic bodies. Phys. Rev. A 39, 5932–5948.
Southern, E., Thomas, A.G., 1965. Effect of constraints on the equilibrium swelling of rubber vulcanizates. J. Polym. Sci. A 3, 641–646.
Sultan, E., Boudaoud, A., 2008. The buckling of a swollen thin gel layer bound to a compliant substrate. J. Appl. Mech. 75, 051002.
Tanaka, H., Tomita, H., Takasu, A., Hayashi, T., Nishi, T., 1992. Morphological and kinetic evolution of surface patterns in gels during the swelling process: evidence of dynamic pattern ordering. Phys. Rev. Lett. 68, 2794–2797.
Tanaka, T., Sun, S.-T., Hirokawa, Y., Katayama, S., Kucera, J., Hirose, Y., et al., 1987. Mechanical instability of gels at the phase transition. Nature 325, 796–798.
Treloar, L.R.G., 1958. The Physics of Rubber Elasticity. Oxford University Press.
Trujillo, V., Kim, J., Hayward, R.C., 2008. Creasing instability of surface-attached hydrogels. Soft Matter 4, 564–569.
Velankar, S.S., Lai, V., Vaia, R.A., 2012. Swelling-induced delamination causes folding of surface-tethered polymer gels. ACS Appl. Mater. Interf. 4, 24–29.
Weiss, F., Cai, S., Hu, Y., Kang, M.K., Huang, R., Suo, Z., Submitted. Creases and wrinkles on the surface of a swollen gel.
Wong, W.H., Guo, T.F., Zhang, Y.W., Cheng, L., 2010. Surface instability maps for soft materials. Soft Matter 6, 5743–5750.